Briefings in Bioinformatics, 22(6), 2021, 1–13

https://doi.org/10.1093/bib/bbab224
Problem Solving Protocol

Likelihood-based tests for detecting circadian rhythmicity and differential circadian patterns in transcriptomic applications

Haocheng Ding, Lingsong Meng, Andrew C. Liu, Michelle L. Gumz, Andrew J. Bryant, Colleen A. Mcclung, George C. Tseng, Karyn A. Esser and Zhiguang Huo

Corresponding author: Zhiguang Huo, Department of Biostatistics, University of Florida, Gainesville, FL, 32608, USA. E-mail: zhuo@ufl.edu

Abstract

Circadian rhythmicity in transcriptomic profiles has been shown in many physiological processes, and the disruption of circadian patterns has been found to associate with several diseases. In this paper, we developed a series of likelihood-based methods to detect (i) circadian rhythmicity (denoted as LR_rhythmicity) and (ii) differential circadian patterns comparing two experimental conditions (denoted as LR_diff). In terms of circadian rhythmicity detection, we demonstrated that our proposed LR_rhythmicity could better control the type I error rate compared to existing methods under a wide variety of simulation settings. In terms of differential circadian patterns, we developed methods in detecting differential amplitude, differential phase, differential basal level and differential fit, which also successfully controlled the type I error rate. In addition, we demonstrated that the proposed LR_diff could achieve higher statistical power in detecting

Haocheng Ding is a PhD candidate in the Department of Biostatistics at the University of Florida. His research interest includes developing statistical methodology for circadian analysis and differential circadian analysis.
Lingsong Meng is a PhD candidate in the Department of Biostatistics at the University of Florida. His research interest includes genomic applications in identifying circadian rhythmicity and differential circadian patterns.
Dr Andrew C. Liu is an Associate Professor in the Department of Physiology and Functional Genomics at the University of Florida College of Medicine. The major focus of his lab is to study the molecular, cellular and physiological mechanisms of circadian clocks in mammals.
Dr Michelle L. Gumz is an Associate Professor in the Division of Nephrology, Hypertension and Renal Transplantation in the Department of Medicine at the University of Florida. She is interested in the clinical implications of circadian rhythms in human health, particularly kidney function.
Dr Andrew J. Bryant is an Assistant Professor in the Division of Pulmonary, Critical Care and Sleep Medicine in the Department of Medicine at the University of Florida. He is interested in the role of circadian influence on leukocyte activation and involvement in pulmonary hypertension secondary to fibrosis or emphysema.
Dr Colleen A. McClung is a Professor of Psychiatry and Clinical and Translational Science at the University of Pittsburgh. She is interested in studying the association between circadian clock and various psychiatric disorders, including bipolar disorder, major depression and drug addiction.
Dr George C. Tseng is a Professor in the Department of Biostatistics at the University of Pittsburgh. His research group focuses on developing rigorous, timely and impactful methodologies in the area of genomics and bioinformatics, to help understand disease mechanisms and improve disease diagnosis and treatment.
Dr Karyn A. Esser is a Professor in the Department of Physiology and Functional Genomics at the University of Florida College of Medicine. Her lab focuses research on the role of circadian rhythms and the molecular clock mechanism in skeletal muscle homeostasis and health.
Dr Zhiguang Huo is an Assistant Professor in the Department of Biostatistics at the University of Florida. His research interest includes developing statistical and machine learning methodology for the broad field of genomics and bioinformatics.
Submitted: 11 February 2021; **Received (in revised form):** 06 May 2021

differential fit, compared to existing methods. The superior performance of LR_rhythmicity and LR_diff was demonstrated in four real data applications, including a brain aging data (gene expression microarray data of human postmortem brain), a time-restricted feeding data (RNA sequencing data of human skeletal muscles) and a scRNAseq data (single cell RNA sequencing data of mouse suprachiasmatic nucleus). An R package for our methods is publicly available on GitHub https://github.com/diffCircadian/diffCircadian.

Key words: circadian rhythmicity; differential circadian analysis; gene expression; likelihood-based test; R package; comparison study.

INTRODUCTION

Circadian rhythms are an endogenous ∼24 hours cycle of behavior and physiology including sleep–wake cycles, body temperature and melatonin [1, 3, 7, 19]. Underlying circadian rhythms is the clock mechanism that is found in virtually all cells of body. This mechanism is defined by a transcriptional-translational feedback loop involving a set of core clock genes [11, 18], including *CLOCK*, *BMAL1*, period family (*PER1*, *PER2*, *PER3*) and cryptochrome family (*CRY1*, *CRY2*). Beyond the core clock mechanism, genome-wide transcriptomic studies have uncovered circadian genes expression patterns in many tissues, including postmortem brain [4, 33], skeletal muscle [12], liver [15] and blood [26]. Zhang *et al.* [46] and Ruben *et al.* [31] conducted genome-wide circadian analyses using transcriptomic data of 12 unique mouse organs and 13 unique human organs, respectively, and showed that the profiles of circadian gene expression were tissue specific. It is now recognized from studies in humans and rodents that disruption in clock and circadian gene expression are linked to diseases including type II diabetes [35], sleep [26], major depression disease [22], aging [4], schizophrenia [33] and Alzheimer's disease [23].

In the literature, several algorithms have been developed to detect circadian rhythmicity, including F-test via cosinor-based rhythmometry [5], Lomb-Scargle periodograms [10], COSOPT [36], ARSER [44], RAIN [38], JTK CYCLE [16] and MetaCycle [43]. These algorithms were widely applied in transcriptomic studies, and the comparisons of these algorithm have been evaluated in several review studies [14, 21, 25]. Though promising, concerns have been raised [21] that the *P*-values generated by many of these existing methods may not be correct (i.e. do not follow a uniform distribution [i.e. $U(0, 1)$] under the null), implying a potential inflated or deflated type I error rate.

Another increasingly important research question is to identify differential circadian patterns associated with different experimental conditions [13, 17, 26]. Figure 1 shows four types of differential circadian patterns identified in our brain aging data application (see Section 4.1 for details), among which 31 subjects were from the young group (age $\leq$ 40 years), and 37 subjects were from the old group (age $>$ 60 years). Gene *CIART* in Figure 1A shows the differential amplitude, where the amplitude in the young group is larger than the old group; Gene *PER2* in Figure 1B shows the differential phase, where the phases in young and old groups are different; Gene *TRIB2* in Figure 1C shows the differential basal level, where the basal level in the young group is higher than the old group; Gene *MYO5A* in Figure 1D shows the differential fit, where there exists a good circadian rhythmicity fit in the young group, but not in the old group. The definition of amplitude, phase, and basal level is illustrated in Figure 2. The traditional approach to compare circadian rhythmicity between two experimental conditions is to adopt a hard threshold (e.g. $P \leq 0.01$) as the significance cutoff, and then declare deferential circadian rhythmicity if a gene is significant in only one condition [26, 30]. Though straightforward, this approach may fail under the following two scenarios. Scenario (i): gene *PER2* in Figure 1B is showing significant circadian rhythmicity in both the young group ($P = 1.60\times10^{-4}$) and the old group ($P = 7.37\times10^{-5}$), and thus did not satisfy the definition of differential circadian pattern. However, Figure 1B shows a clear phase difference comparing young and old groups, and the underlying differential phase *P*-value using our proposed method was 5.43×10^{-5}. Scenario (ii): gene *EEF2K* had a circadian *P*-value 0.0096 in the young group, and a *P*-value 0.0305 in the old group. Though this gene satisfied this definition of differential circadian pattern using $P \leq 0.01$ as the significance criteria, the rhythmicity *P*-values under both conditions were close to 0.01. In fact, the resulting differential fit *P*-value using our proposed method was 0.709, indicating *EEF2K* was not showing differential circadian pattern comparing the young group and the old group.

In the literature, some methods have been developed to identify genes showing differential circadian patterns. Chen *et al.* [4] developed a permutation test to quantify the statistical significance of these four types of differential circadian patterns. However, the non-parametric permutation test could suffer from low *P*-value precision and heavy computational burdens. DODR [39] and LimoRhyde [34] were developed to examine the hypothesis that the circadian rhythmicity across two conditions are identical, but they failed to further categorize different subclasses of differential circadian patterns illustrated in Figure 1. More recently, circaCompare [29] was developed to detect differential amplitude, differential phase and differential basal level using non-linear least square methods, but it could not characterize differential fit. To our knowledge, there is still a lack of unified parametric method that could identify all four differential circadian patterns simultaneously. In addition, the performance of these existing methods has not been systematically evaluated.

In the statistics field, likelihood-based methods enjoyed tremendous popularity for its simplicity when testing single parameter and its flexibility to extend to test multiple parameters or complex models. In addition, the testing procedures based on the likelihood-based methods are generally considered as asymptotically the most efficient. However, this concept has not been fully developed in the field of circadian analysis. To close these research gaps, and to fully incorporate the merit of likelihood-based approaches, we propose a series of likelihood-based methods to detect circadian rhythmicity (within one condition) as well as differential circadian patterns (comparing two conditions). The contribution and novelty of this paper includes the following: (i) systematically evaluated the accuracy of *P*-values in detecting circadian rhythmicity of our likelihood-based methods and other existing methods; (ii) the first to propose likelihood-based methods to identify all four types of differential circadian patterns; (iii) systemically evaluated our likelihood-based methods in detecting differential circadian

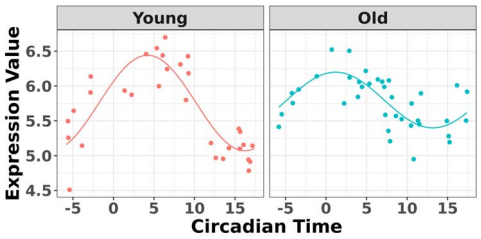

(a) Differential amplitude for $CIART$ ($p = 0.008$)

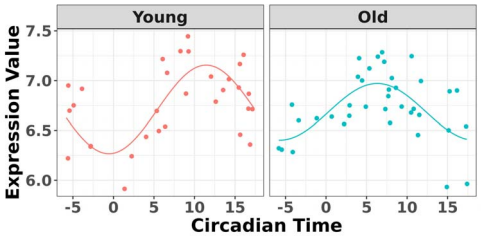

(b) Differential phase for $PER2$ ($p = 5.43 \times 10^{-5}$)

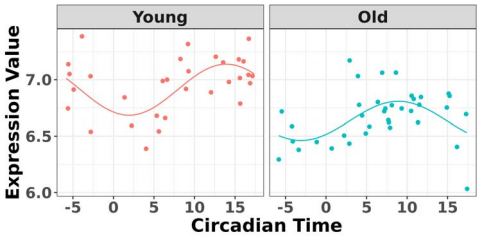

(c) Differential basal level for $TRIB2$ ($p = 2.88 \times 10^{-6}$)

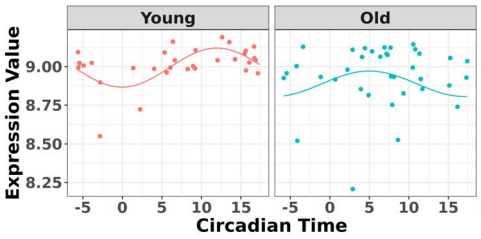

(d) Differential fit for $MYO5A$ ($p = 4.34 \times 10^{-8}$)

FIGURE 1. The most significant genes showing four types of differential circadian patterns from the brain aging data.

patterns, and compared with existing methods in terms of the correctness of P-value and statistical power; (iv) implemented our proposed methods in R software package, which has been made publicly available on GitHub.

METHOD

We developed likelihood-based methods for (i) circadian rhythmicity detection within one experimental condition and (ii) differential circadian pattern analysis comparing two experimental conditions. The statistical inference of these methods were based on the Wald statistics and the likelihood ratio statistics. Since the accurate inference of the likelihood-based methods required large sample size, we also employed finite sample corrections to improve the performance under small sample sizes.

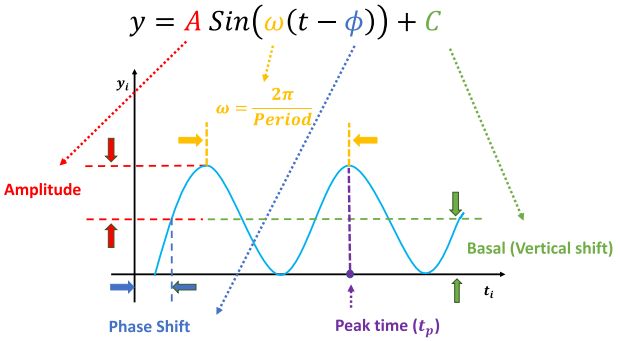

FIGURE 2. Illustration of a sinusoidal wave fitting and its related terminologies.

Notations for a sinusoidal wave fitting

Our methods assume that the relationship between the gene expression level and the circadian time fits a sinusoidal wave curve. As illustrated in Figure 2, denote y as the expression value for a gene; t as the circadian time; C as the basal level (vertical shift of the sinusoidal wave baseline from 0); A as the amplitude. ω is the frequency of the sinusoidal wave, where $\omega = \frac{2\pi}{Period}$. Without loss of generality, we set $period = 24$ hours to mimic the diurnal period. ϕ is the phase of the sinusoidal wave curve. Whenever there is no ambiguity, we will omit the unit 'hours' in period, phase, and other related quantities. Due to the periodicity of a sinusoidal wave, (ϕ_1, ϕ_2) are not identifiable when $\phi_1 = \phi_2 + 24$. Therefore, we will restrict $\phi \in [-6, 18)$. ϕ may be difficult to read from a sinusoidal wave (Figure 2), and a closely related quantify is the peak time t_P. The connection between ϕ and t_P is that $\phi + t_P = 6 \pm 24N$, where N is an arbitrary natural number.

Circadian rhythmicity detection

In this section, we develop likelihood-based methods to test the existence of a circadian rhythmicity within one experimental condition. Denote y_i is the expression value of one gene for subject $i (1 \le i \le n)$, where n is the total number of subjects. t_i is the circadian time for subject i. We assume

$$y_i = A\sin(\omega(t_i + \phi)) + C + \varepsilon_i, \tag{1}$$

where ε_i is the error term for subject i; we assume ε_i's are identically and independently distributed (i.e. iid) and $\varepsilon_i \sim N(0, \sigma^2)$, where σ is the noise level. To benchmark the goodness of sinusoidal wave fitting, we define the coefficient of determination $R^2 = 1 - \frac{RSS}{TSS}$, where $RSS = \sum_{i=1}^{n}(y_i - \hat{y}_i)^2$, $TSS = \sum_{i=1}^{n}(y_i - \bar{y})^2$, $\hat{y}_i = \hat{A}\sin(\omega(t_i + \hat{\phi})) + \hat{C}$, $\bar{y} = \sum_i y_i/n$, with $\hat{A}$, $\hat{\phi}$ and $\hat{C}$ being the fitted value for A, ϕ and C in Equation 1 under least square loss, respectively. R^2 ranges from 0 to 1, with 1 indicating perfect sinusoidal wave fitting, and 0 indicating no fitting at all. Based on these assumptions, we derive procedures for testing circadian rhythmicity. For the ease of discussion, we re-write Equation 1 as

$$y_i = E\sin(\omega t_i) + F\cos(\omega t_i) + C + \varepsilon_i, \tag{2}$$

where $E = A\cos(\omega\phi)$, and $F = A\sin(\omega\phi)$. The hypothesis setting for testing the existence circadian rhythmicity is $H_0 : E = F = 0$ *v.s.* $H_A : E \neq 0$ or $F \neq 0$. We will derive the Wald statistics and the likelihood ratio statistics to perform hypothesis testing. Since both Wald statistics and likelihood ratio statistics are

designed based on large sample theories, we will also employ finite sample statistics for these methods.

Likelihood ratio test

Based on Equation 2, the likelihood function of all n samples is

$$\begin{aligned} & L(E, F, C, \sigma^2) \\ &= \prod_{i=1}^{n} L_i(E, F, C, \sigma^2 | y_i, t_i) \\ &= \prod_{i=1}^{n} \frac{1}{\sqrt{2\pi\sigma^2}} \exp\left(-\frac{(y_i - E\sin(\omega t_i) - F\cos(\omega t_i) - C)^2}{2\sigma^2}\right) \end{aligned}$$

The log-likelihood function is

$$\begin{aligned} & l(E, F, C, \sigma^2) \\ &= \log L(E, F, C, \sigma^2) \\ &= -\frac{n}{2}\log(2\pi\sigma^2) - \sum_{i=1}^{n} \frac{(y_i - E\sin(\omega t_i) - F\cos(\omega t_i) - C)^2}{2\sigma^2} \end{aligned}$$

Under H_0, $\boldsymbol{\beta} = \boldsymbol{\beta}_0 = (0, 0, \hat{C}_0, \hat{\sigma}_0^2)^\top$, and $l_0 = l(0, 0, \hat{C}_0, \hat{\sigma}_0^2)$, where $\boldsymbol{\beta}_0$ is the least square estimate of Equation 2 under H_0. Under H_A, $\boldsymbol{\beta} = \boldsymbol{\beta}_A = (\hat{E}_A, \hat{F}_A, \hat{C}_A, \hat{\sigma}_A^2)^\top$ and $l_A = l(\hat{E}_A, \hat{F}_A, \hat{C}_A, \hat{\sigma}_A^2)$, where $\boldsymbol{\beta}_A$ is the least square estimate of Equation 2. The likelihood ratio test statistic is: $T^{LR} = -2(l_0 - l_A)$. Since the degree of freedom is 2, under H_0, $T^{LR} \sim \chi_2^2$.

Wald test

The Wald test statistic can be derived as $T^{Wald} = (\boldsymbol{\beta}_A - \boldsymbol{\beta}_0)^\top I(\boldsymbol{\beta}_A)(\boldsymbol{\beta}_A - \boldsymbol{\beta}_0)$, where $I(\boldsymbol{\beta}_A)$ is Fisher information matrix evaluated at $\boldsymbol{\beta}_A$. Under H_0, $T^{Wald} \sim \chi_2^2$.

Finite sample Wald/LR tests

The Wald test and the likelihood ratio test may have inflated type I error when sample size is small since they rely on large sample asymptotic theory. Parker [28] introduced finite sample Wald and likelihood ratio test statistics, which could better control the type I error rate to the nominal level even with small sample sizes. The finite sample Wald statistics (T_{FN}^{Wald}) and the finite sample likelihood ratio statistics (T_{FN}^{LR}) can be derived as the following:

$$T_{FN}^{Wald} = \frac{n-k+1}{nr} T^{Wald} \tag{3}$$

$$T_{FN}^{LR} = \frac{n-k+1}{r}\left(\exp(T^{LR}/n) - 1\right) \tag{4}$$

where $k = 4$ is total number of parameters and $r = 2$ is number of parameters of interest. Under the null hypothesis, $T_{FN}^{Wald} \sim F(df_1, df_2)$, and $T_{FN}^{LR} \sim F(df_1, df_2)$, where $df_1 = r$ and $df_2 = n - k + 1$.

F-test

The F-test method to detect the circadian rhythmicity has been previously established [5]. F-test constructs its test statistic by decomposing total variability into model sum of square, and residual sum of square, which is closely related to our proposed finite sample likelihood method. Thus, we also describe the F-test method in our manuscript and will draw connection between F-test and our likelihood method.

$$T^F = \frac{(TSS - RSS)/df_1}{RSS/df_2} \sim F(df_1, df_2),$$

where residual sum of squares $(RSS) = \sum_{i=1}^{n}(y_i - \hat{y}_i)^2$, total sum of squares $(TSS) = \sum_{i=1}^{n}(y_i - \bar{y})^2$, $df_1 = 2$ and $df_2 = n - 3$. Under the null hypothesis, $T^F \sim F(df_1, df_2)$.

Other competing methods

We will compare our proposed likelihood-based method to other existing methods, including F-test [5], ARSER [44], Lomb–Scargle periodograms [10], JTK CYCLE [16], RAIN [38], MetaCycle [43] and the permutation test [4]. ARSER, RAIN, JTK CYCLE and MetaCycle have some special requirement for the input circadian time—the input circadian time has to be integer value, and the intervals between two adjacent circadian time points must be the same. Thus, we will accommodate such design in our simulation settings when needed.

Differential circadian analysis

In this section, we develop likelihood-based testing procedures to identify genes showing differential circadian patterns, including (i) differential amplitude, (ii) differential phase, (iii) differential basal level and (iv) differential fit, as shown in Figure 1.

Denote y_{1i} as the gene expression value of subject $i (1 \le i \le n_1)$ in experimental condition 1, where n_1 is the total number of subjects; t_{1i} is the circadian time for subject i; y_{2j} is the gene expression value of subject $j (1 \le j \le n_2)$ in experimental condition 2, where n_2 is the total number of subjects; t_{2j} is the circadian time for subject j. Note that y_{1i} and y_{2j} are from the same gene, but under different experimental conditions. We assume the following models:

$$\begin{aligned} y_{1i} &= A_1 \sin(\omega(t_{1i} + \phi_1)) + C_1 + \varepsilon_{1i} \\ y_{2j} &= A_2 \sin(\omega(t_{2j} + \phi_2)) + C_2 + \varepsilon_{2j} \end{aligned} \tag{5}$$

$\varepsilon_{1i} \sim N(0, \sigma_1^2)$ is the error term for subject i $(1 \le i \le n_1)$ for experimental condition 1 and $\varepsilon_{2j} \sim N(0, \sigma_2^2)$ is the error term for subject j $(1 \le j \le n_2)$ for experimental condition 2. These error terms are assumed to be iid. A_1, ϕ_1, C_1 and σ_1^2 are the amplitude, phase, basal level and noise level for the experimental condition 1, and A_2, ϕ_2, C_2 and σ_2^2 are for experimental condition 2.

Hypothesis testing framework for differential circadian analysis

Below we state the null hypothesis and the alternative hypothesis for testing these four categories of differential circadian patterns, based on Equation 5.

1. Differential amplitude: $H_0 : A_1 = A_2 = A_c$ *v.s.* $H_A : A_1 \ne A_2$.
2. Differential phase: $H_0 : \phi_1 = \phi_2 = \phi_c$ *v.s.* $H_A : \phi_1 \ne \phi_2$.
3. Differential basal level: $H_0 : C_1 = C_2 = C_c$ *v.s.* $H_A : C_1 \ne C_2$.
4. Differential fit: $H_0 : \sigma_1^2 = \sigma_2^2 = \sigma_c^2$ *v.s.* $H_A : \sigma_1^2 \ne \sigma_2^2$.

We have several remarks on our procedure. (i) As suggested by Chen *et al.* [4], the circadian rhythmicity can be characterized by the goodness of fit statistics R^2. Since it is not easy to derive statistical inference on R^2, we will use a closely related quantity, σ^2, to quantify the goodness of fit. (ii) The prerequisite for differential amplitude, differential phase, and differential basal level is

that there should exist circadian rhythmicity in both conditions under comparisons. Therefore, we suggested users to set $P \leq 0.01$ or $P \leq 0.05$ from our previous likelihood-based circadian rhythmicity test to ensure the existence of the circadian rhythmicity in both conditions. (iii) The prerequisite for differential fit is that there should exist a circadian rhythmicity in either experimental conditions. We suggested users to set $P \leq 0.01$ or $P \leq 0.05$ from our previous likelihood-based circadian rhythmicity test to ensure such prerequisite.

Likelihood ratio test

Based on Equation 5, the log-likelihood function for $n_1 + n_2$ samples in both experimental conditions is as follows:

$$\begin{aligned} & ll(A_1, \phi_1, C_1, \sigma_1^2, A_2, \phi_2, C_2, \sigma_2{}^2) \\ &= \sum_{i=1}^{n_1} l_i(A_1, \phi_1, C_1, \sigma_1{}^2) + \sum_{j=1}^{n_2} l_j(A_2, \phi_2, C_2, \sigma_2{}^2) \\ &= \left(-\frac{n_1}{2} \log \sigma_1{}^2 - \sum_{i=1}^{n_1} \frac{(y_i - A_1 \sin(\omega(t_i + \phi_1)) - C_1)^2}{2\sigma_1{}^2} \right) \\ &+ \left(-\frac{n_2}{2} \log \sigma_2{}^2 - \sum_{j=1}^{n_2} \frac{(y_j - A_2 \sin(\omega(t_j + \phi_2)) - C_2)^2}{2\sigma_2{}^2} \right) \end{aligned} \quad (6)$$

The test statistic is the following: $D^{LR} = -2(ll_0 - ll_A)$, where ll_0 is the log likelihood under H_0; and ll_A is the log likelihood under H_A. Here the null can be one of the following: (i) $H_0{}^{(a)}$: $A_1 = A_2$ for differential amplitude; (ii) $H_0{}^{(p)}$: $\phi_1 = \phi_2$ for differential phase; (iii) $H_0{}^{(b)}$: $C_1 = C_2$ for differential basal level; (iv) $H_0{}^{(f)}$: $\sigma^{2_1} = \sigma^{2_2}$ for differential fit. For all these null hypotheses, the degree of freedom is 1, and $D^{LR} \sim \chi^{2_1}$ under H_0. For example when testing different amplitude, under $H_0^{(a)}$, $\hat{A_1} = \hat{A_2} = \hat{A}_c$, $ll_0 = ll(\hat{A}_c, \hat{\phi}_1, \hat{C}_1, \hat{\sigma}_1, \hat{A}_c, \hat{\phi}_2, \hat{C}_2, \hat{\sigma}_2 | y)$; and under $H_A^{(a)}$, $\hat{A_1} \neq \hat{A_2}$, $ll_A = ll(\hat{A_1}, \hat{\phi}_1, \hat{C}_1, \hat{\sigma}_1, \hat{A_2}, \hat{\phi}_2, \hat{C}_2, \hat{\sigma}_2 | y)$.

Wald test

Denote $\boldsymbol{p} = (A_1, \phi_1, C_1, \sigma_1{}^2, A_2, \phi_2, C_2, \sigma_2^2)^\top$. $\boldsymbol{p}_0$ is $\boldsymbol{p}$ under H_0, where H_0 is one of the null hypotheses in Section 2.3.1; $\boldsymbol{p}_1$ is $\boldsymbol{p}$ under H_A, where there is no restriction on $\boldsymbol{p}$. Then the Wald test statistic is $D^{Wald} = (\boldsymbol{p}_1 - \boldsymbol{p}_0)^\top I(\boldsymbol{p}_1)(\boldsymbol{p}_1 - \boldsymbol{p}_0)$. Under H_0, $D^{Wald} \sim \chi_1^2$, where $I(\boldsymbol{p}_1)$ is Fisher information matrix evaluated at $\boldsymbol{p}_1$.

Finite sample Wald/LR tests

Again, in order to control type I error for small sample sizes, we derive finite sample version of the Wald statistics and likelihood ratio statistics D_{FN}^{Wald} and D_{FN}^{LR} by Equations 3 and 4. Under H_0, $D_{FN}^{Wald} \sim F(df_1, df_2)$, and $D_{FN}^{LR} \sim F(df_1, df_2)$, where $df_1 = r$ and $df_2 = n - k + 1$.

Competing methods for differential circadian analysis

We will compare the performance of our method with other existing methods, including the permutation test [4], DODR [39], LimoRhyde [34] and circaCompare [29]. We acknowledge that HANOVA, robustDODR and LimoRhyde are designed to detect differential rhythmicity (i.e. whether the circadian rhythmicity across two conditions are identical) and cannot distinguish the four subcategories in Figure 1. Thus we will apply these two methods in detecting differential fit, which is closely related to differential rhythmicity conceptually; circaCompare can examine differential amplitude, differential phase and differential basal level, while the permutation test as well as our proposed method can examine all four types if differential circadian patterns illustrated in Figure 1.

Computational consideration

Parameter estimations for Equation 1 were performed by the nonlinear least square algorithm in R package *minpack.lm* [9]. In addition, for differential circadian analysis, we used optimization method in R package *nloptr* [45] for parameter estimation in Equation 6.

SIMULATION

In terms of circadian rhythmicity detection, we demonstrated that our proposed method correctly controlled the type I error rate to the nominal level, while some of the other methods failed to control the type I error rate. In terms of differential circadian pattern detection, our method still controlled the type I error rate to the nominal level. For differential fit, which is one type of the differential circadian pattern shown in Figure 1b, we demonstrated our method achieved higher statistical power compared to the existing methods.

Simulation for circadian rhythmicity analysis

Simulation settings

Denote $i (1 \leq i \leq n)$ as the sample index, where n was the total number of samples. The circadian time t_i for sample i was generated from uniform distribution UNIF$(0, 24)$. We simulated the gene expression value for sample i using Equation 1.

$$y_i = A \sin(\omega(t_i + \phi)) + C + \varepsilon_i.$$

Our basic parameter setting for simulation is listed as below. For each gene, the sample size n was set to be 12; the circadian time were sampled every 2 hours (i.e. $t_1 = 1$, $t_2 = 3$, ..., $t_{12} = 23$), such integer circadian time and evenly spaced interval time are required by some other existing methods. Whenever the statistical methods have no such requirement, we sampled circadian time directly from UNIF$(0, 24)$. Amplitude A was fixed at 1; phase ϕ was generated from UNIF$(0, 24)$. Basal level C was generated from UNIF$(0, 3)$. Error term ε_i was generated from normal distribution $N(0, \sigma^2)$ where σ^2 was set to be 1. We simulated $G = 10\,000$ genes for each simulation, and each simulation was repeated $B = 10$ times to increase numbers of replications and to obtain an standard deviation estimate. To examine whether our method is robust against higher signal-noise ratios, correlated gene structures and violations of normality distributions, we further simulates the following variations:

1. Impact of sample sizes. We varied $n = 6, 12, 24, 48, 96$ while fixing other parameters in the basic parameter setting fixed. Note that when $n > 24$, we would allow repetitive circadian time for different samples. For example, when $n = 48$, the circadian time sequence would be $t_1 = 1$, $t_2 = 1$, $t_3 = 2$, ..., $t_{47} = 24$ and $t_{48} = 24$.
2. Impact of signal noise ratio. The signal noise ratio is defined as $\frac{A}{\sigma}$. Thus we varied $\sigma = 1, 2, 3$ to mimic varying levels of signal noise ratio, while fixing other parameters in the basic parameter setting.

3. Impact of correlated genes. In transcriptomic data applications, individual genes can be correlated. Thus, we simulated the following correlated structure. For every m = 50 genes, we simulated

$$\mathbf{y} = A\sin(\omega(\mathbf{t}+\phi)) + C + \boldsymbol{\varepsilon},$$

where $\mathbf{y} = (y_1, \ldots, y_m)$, $\mathbf{t} = (t_1, \ldots, t_m)$ and $\boldsymbol{\varepsilon} = (\varepsilon_1, \ldots, \varepsilon_m)$. In this case, $\boldsymbol{\varepsilon}$ were generated from a multivariate normal distribution $MVN(0, \boldsymbol{\Sigma})$. And $\boldsymbol{\Sigma} \in \mathbb{R}^{m\times m}$ was the covariance matrix generated from the inverse Wishart distribution $W^{-1}(\boldsymbol{\Phi}, \upsilon)$. In order to mimic correlated gene structure, we first designed $\Phi' = (1-\rho)I_{m\times m} + \rho J_{m\times m}$ and then standardized Φ' to correlation matrix Φ, where $I_{m\times m}$ was the identify matrix, and $J_{m\times m} \in \mathbb{R}^{m\times m}$ a matrix with all elements 1. We fixed υ to be 60, and vary $\rho = 0, 0.25, 0.5$.
4. Violation of the Gaussian assumption. Instead of assuming the error term was generated from a standard normal distribution (i.e. $N(0,1)$), we generated $\varepsilon_1 \sim t(3), t(5), t(10), t(\infty)$, where $t(df)$ is the t-distribution with degree of freedom df. This family of t-distributions represents long-tailed error distribution, with smaller df indicating longer tailed error distribution, and thus larger violation of the normality assumption. When $df = \infty$, $t(\infty)$ is the same as $N(0,1)$.

The best performer of the likelihood based methods in detecting circadian rhythmicity

Before comparing with other existing methods, we first evaluated the type I error rate (nominal α level 5%) of our proposed four likelihood-based methods in detecting circadian rhythmicity, including Wald test (regular), Wald test (finite sample), likelihood ratio test (regular) and likelihood ratio test (finite sample). Since the limiting distribution of both Wald statistics (finite sample) and likelihood ratio statistics (finite sample) follows an F-distribution, we also include the F-test method [5] as benchmark.

Figure S2 showed type I error rates (nominal α level 5%) of our proposed four methods and the F-test method. Regardless of the varying sample sizes, the Wald test (finite sample), the likelihood ratio test (finite sample) and the F-test controlled the type I error rate close to the 5% nominal level, while the Wald test (regular) and the likelihood ratio test (regular) obtained inflated type I error rate. The Wald test (regular) and the likelihood ratio test (regular) had better performance when sample size became larger, which was not unexpected because these asymptotic tests rely on large sample sizes. Remarkably, we observed that the Wald test (finite sample) and the likelihood ratio test (finite sample) achieved almost the same test statistics as the F-test, indicating the finite sample approximation procedure [28] successfully convert our likelihood-based statistics to F-statistics.

Similar results was also observed by varying signal noise ratio (Figure S3) and varying the strength of gene correlations (Figure S4). The Wald test (finite sample), the likelihood ratio test (finite sample) and the F-test could better control the type I error rate to the 5% nominal level compared to the Wald test (regular) and the likelihood ratio test (regular).

As shown in Figure S5, when we varied the level of normality violation by varying df of the t-distribution, we observed that all test procedures became slightly more conservative.

In particular, for the likelihood ratio test (finite sample), when these was a slight (df=10) or moderate (df=5) violation of the normality assumption, this method still controlled the type I error rate well ($0.049 \sim 0.046$). When there was severe (df=3) violation of the normality assumption, the type I error rate was still 0.043, which was not far away from the nominal 5% level. These results indicate our method is robust against normality assumptions. In practice, if the residuals (i.e. $y_i - \hat{y}_i$) violated the Gaussian distribution, we would recommend data transformations (e.g. Box–Cox transformation [2]) to improve normality. In supplementary material Section 1, we included a concrete simulated example to demonstrate how to use the Box–Cox transformation to rescue the normality assumption under the setting of detecting circadian rhythmicity.

To summarize, the Wald test (finite sample) and the likelihood ratio test (finite sample) are the best performer of our proposed likelihood-based methods in detecting circadian rhythmicity, which could control the type I error rate to the nominal level under the Gaussian assumption. And these two methods are equivalent to the F-test method in terms of the test statistics. Therefore, we will pick up the likelihood ratio test (finite sample) as the representative of our proposed methods in detecting circadian rhythmicity, and we denoted LR_rhythmicity as the short name for this method in all later evaluations.

Type I error rate comparison with other methods

We compared the likelihood-based method (LR_rhythmicity) with other existing methods in detecting circadian rhythmicity, including Lomb-Scargle, JTK, ARSER, Rain, MetaCycle and the permutation test. We excluded the F-test in our evaluation, since it is essentially the same as LR_rhythmicity. Figure 3 showed type I error rates by varying sample sizes. In general, LR_rhythmicity and the permutation test controlled the type I error rate to the 5% nominal level, while the other methods had inflated or deflated type I error rate. Similar results were also observed by varying signal noise ratio (Figure S6) and varying the strength of gene correlations (Figure S7). As shown in Figure S8, we observed that violation of normality assumption will lead to a slightly smaller than expected type I error rate for LR_rhythmicity.

To summarize, under the Gaussian assumption (i.e. the residuals follow normal distribution), only the LR_rhythmicity and the permutation test can achieve nominal type I error rate control (i.e. 5%). And when there is a violation of the Gaussian assumption, LR_rhythmicity is robust and we only observed a slight deviation of the type I error rate.

These type I error rates ranged from 0.038 to 0.048, which were close to the nominal 5% level. indicating our method is robust against normality assumptions.

Power analysis

For the power analysis, we only examined the method that could successfully control the type I error rate to the 5% nominal level. Otherwise, the power is directly not comparable because it cannot be distinguished whether a higher/lower power is a result of the test procedure itself, or because of inflated/deflated type I error rate control. Only the LR_rhythmicity and the permutation test survived these criteria. Figure S9 shows the power with respect to varying sample sizes. Both these methods are similarly powerful at 5% nominal level of type I error rate. When the sample size is larger, both tests became more powerful. However, we want to point out that the precision of the permutation test depends heavily on the number of permutations. For example, it may need at least 1,000,000 permutations in order to achieve a $P < 10^{-6}$, which could be a computational burden. The LR_rhythmicity has no such restriction and could obtain an arbitrarily small P-values without extra computational concerns.

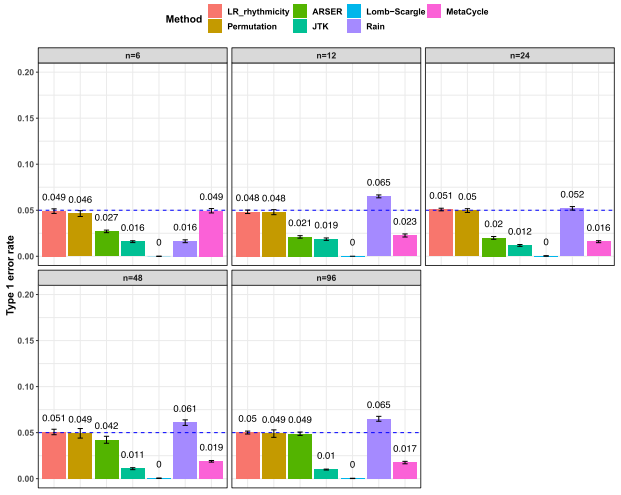

FIGURE 3. Type I error rate at nominal α level 5% for 7 different methods in detecting circadian rhythmicity. The sample sizes were varied at n=6, 12, 24, 48 and 96. The blue dashed line is the 5% nominal level. A higher than 5% blue dashed line bar indicates an inflated type I error rate; a lower than 5% blue dashed line bar indicates a smaller than expected type I error rate; and a bar at the blue dashed line indicates an accurate type I error rate (i.e. P = 0.05). The standard deviation of the mean type I error rate was also marked on the bar plot.

Sensitivity analysis

To examine how the perturbations of the model parameters affected our results, we further performed sensitivity analysis. Based on the basic simulation settings in previous sections, we varied $A = 1, 2, 3$; $\phi = 1, 2, 3$; $C = 1, 2, 3$; and $\sigma^2 = 1, 2, 3$. As shown in Table S1, the type I error control remained the same regardless of the perturbation in A, ϕ, C and σ^2. In terms of the power, we observed that ϕ and C had no impact. A and σ^2 had an impact on the power, which was not unexpected because A and σ^2 are directly related to the goodness of fit of a circadian curve.

Differential circadian analysis

In this section, we used simulation to evaluate the performance of the likelihood-based method in detecting differential circadian patterns, including differential amplitude, differential phase, differential basal level and differential fit. We first compared among our proposed likelihood-based methods including Wald test (regular), Wald test (finite sample), likelihood ratio test (regular) and likelihood ratio test (finite sample). We found that likelihood ratio test (finite sample) was the best performer of our proposed methods. We then compared this best performer with other existing methods for differential circadian pattern analysis, including Circacompare, limorhyde, HANOVA, robustDODR and the permutation test under variety of simulation settings.

Simulation settings

The simulation setting is based on Equation 5. The basic parameter setting for simulation is listed as below. We set number of genes $G = 10\,000$ and the sample size n was set to be 10. For each gene g ($1 \leq g \leq G$), amplitudes $A_1 = A_2$ were set to be 3; phases $\phi_1 = \phi_2$ were generated from UNIF(0, 24). Basal levels $C_1 = C_2$ were generated from UNIF(10, 13). Error terms $\varepsilon_i, \varepsilon_j$ were generated from normal distribution $N(0, \sigma_1^2)$ and $N(0, \sigma_2^2)$, respectively. $\sigma_1^2 = \sigma_2^2$ were set to be 1. This simulation was repeated 10 times to increase numbers of replications and to obtain standard deviation estimate. To examine the impact of sample size, correlation between genes and distribution violations, we further simulated the following variations.

1. Impact of sample sizes. We varied $n = 10, 20, 50$ while fixing other parameters in the basic parameter setting.
2. Impact of correlated genes. For every m = 50 genes, we simulated the correlated gene structure as described in Section 3.1.1. We varied the strength of correlation $\rho = 0, 0.25, 0.5$ while fixing other parameters in the basic parameter setting.
3. Violation of the Gaussian assumption. As described in Section 3.1.1, we varied the error distribution $\varepsilon_1 = \varepsilon_2 \sim t(3), t(5), t(10), t(\infty)$ to mimic different levels of violation of normality assumptions.

The best performer of the likelihood-based methods in detecting differential circadian patterns

We evaluated the type I error rate (nominal α level 5%) of our proposed likelihood-based methods, including Wald test (regular), Wald test (finite sample), likelihood ratio test (regular) and likelihood ratio test (finite sample), under all pre-mentioned simulation settings. Figures S10 and S11 show that the likelihood ratio test (finite sample) had the best performance in terms of type I error rate control with varying sample size or strength of correlation among genes. Thus, we denoted this method as LR_diff and will further compared LR_diff with other existing methods. In Figure S12, when there was a violation of the Gaussian assumption, we observed that LR_diff still controlled the type I error rate for differential amplitude, differential phase and differential basal levels but resulted in inflated type I error rate of differential fit. This is not unexpected since likelihood-based methods utilized the Gaussian assumption to derive the test statistics. Under this situation, we would recommend users to take transformation (i.e. Box–Cox transformation) to improve normality (see Section 5 for more discussions).

Type I error rate comparison with other methods

We evaluated the type I error rate (nominal α level 5%) of the following methods: LR_diff, Circacompare, limorhyde, HANOVA, robustDODR and permutation test under different simulation settings (See Section 3.2.1 for details). Here, LR_diff and the permutation test are applicable for testing all four types of differential circadian analysis in Figure 1; HANOVA, robustDODR and LimoRhyde are designed to detect differential rhythmicity (i.e. whether the circadian rhythmicity across two conditions are identical) and cannot distinguish the four subcategories. Thus, we will apply these three methods in detecting differential fit, which is closely related to differential rhythmicity conceptually, and Circacompare is applicable for testing differential amplitude, differential phase and differential basal levels (Also see Table 1 for their applicability).

1. Impact of sample sizes. Based on the basic parameter setting, we varied $n = 10, 20, 50$. Figure 4 shows the type I error rate control for the 6 methods. Among which three methods were applicable for detecting differential amplitude, differential basal level and differential phase, including LR_diff, Circacompare and the permutation test. All these three methods could control the type I error rate to the 5% nominal level, though Circacompare is slightly better than LR_diff and the permutation test. In addition, five methods were applicable for detecting differential fit, including

Table 1. Comparison of LR_diff with other existing methods in detecting differential circadian patterns. ✓ indicates a method is applicable or could control the type I error to the nominal level; ∗ indicates the most powerful method among all applicable methods. – indicates the method could roughly control the type I error to the nominal level, but with a non-negligible deviation

	Differential amp/phase/basal		Differential fit	
	Applicable	Type I error	Applicable	Type I error
LR_diff	✓	✓*	✓	✓*
Permutation	✓	✓*	✓	✓
Circacompare	✓	✓*		
limorhyde			✓	✓
HANOVA			✓	-
robustDODR			✓	-

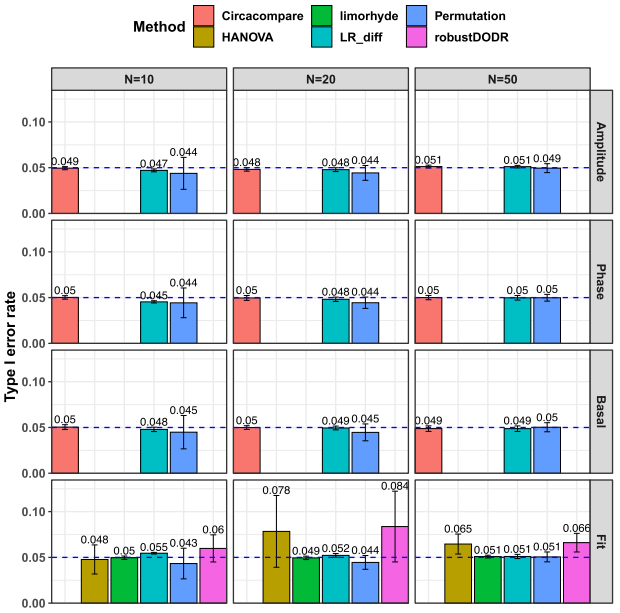

Figure 4. Type I error rate at nominal α level 5% for six different methods in detecting differential circadian patterns. The differential circadian patterns include differential amplitude (Amplitude), differential phase (Phase), differential basal level (Basal) and differential fit (Fit). The sample sizes were varied at N=10, 20 and 50. The blue dashed line is the 5% nominal level. A higher than 5% blue dashed line bar indicates an inflated type I error rate; a lower than 5% blue dashed line bar indicates a smaller than expected type I error rate; and a bar at the blue dashed line indicates an accurate type I error rate (i.e. *P*-value = 0.05). The standard deviation of the mean type I error rate was also marked on the bar plot.

LR_diff, limorhyde, HANOVA, robustDODR and the permutation test. We observed that LR_diff, limorhyde and the permutation test could control the type I error rate to the 5% nominal level, while HANOVA and robustDODR may have slightly inflated type I error rate. We observed their performance did not rely heavily on the sample size, which is expected since these methods did not necessarily rely on large sample size.

2. Impact of correlated genes. Figure S13 shows the type I error rate control by varying the strength of correlations between genes. Similar to the previous simulation setting, we did not observe the correlated gene structure had a big impact on their performance.
3. Violation of the Gaussian assumption. Instead of assuming the error term was generated from a standard normal distribution (i.e. $N(0,1)$), we generated $\varepsilon_1 \sim t(3), t(5), t(10), t(\infty)$, where $t(df)$ was the t-distribution with degree of freedom df. Smaller df represents longer tailed error distribution, and thus larger violation of the normality assumption. Figure S14 shows the type I error rate control for the six methods. In terms of differential amplitude, differential basal level and differential phase, LR_diff, Circacompare and the permutation test successfully controlled the type I error rate to the 5% nominal. In terms of differential fit, we observed that the LR_diff would obtain inflated type I error rate, while the performance of limorhyde, HANOVA, robustDODR and the permutation test were similar regardless of violation of the Gaussian assumption. This is not unexpected because our likelihood-based method relied on the Gaussian assumption to derive its test statistics. Under this situation, we would recommend uses to take transformation (i.e. Box–Cox transformation) to improve normality (see Section 5 for more discussions).

To summarize, in terms of differential amplitude, differential basal level and differential phase, LR_diff, Circacompare and the permutation test could control the type I error rate to the 5% nominal level. In terms of differential fit and under normality assumption, LR_diff, limorhyde and the permutation test could control the type I error rate to the 5% nominal level, while HANOVA and robustDODR may have slightly inflated type I error rate.

Power analysis

In principle, all methods could control the type I error rate to the 5% nominal level, we included all these methods in the power evaluation (Figure 5). In terms of differential amplitude, differential basal level and differential phase, with increasing sample size or larger effect size, all three methods, including LR_diff, Circacompare and the permutation test, became more powerful. Fixing the sample size and effect size, we observed that LR_diff and Circacompare are a little bit more powerful than the permutation test. In terms of differential fit, remarkably, our proposed LR_diff is much more powerful than the permutation test, limorhyde, HANOVA and robustDODR. In addition, with increasing sample size or larger effect size, LR_diff and the permutation test are becoming more powerful, while the other methods remained similar power or had a little bit elevated power. Table 1 summarizes applicability, performance of type I error rate control and power for all these methods.

We observed that our proposed LR_diff had very similar type I error rate and statistical power compared to Circacompare. In fact, both LR_diff and Circacompare were designed to address the same question (i.e. differential amplitude, phase and basal level) by deploying cosinor-based rhythmometry. The difference is that LR_diff utilized a likelihood ratio test, whereas Circacompare employed a non-linear least square approach. In addition, LR_diff is capable of testing different fit, while Circacompare cannot be used to perform this test.

REAL DATA APPLICATIONS

We evaluated our likelihood-based methods (LR_rhythmicity and LR_diff) in four real data applications, including a gene expression microarray data of human postmortem brain (comparing chronological age [i.e. young versus old]), a gene expression RNA sequencing data of human skeletal muscles

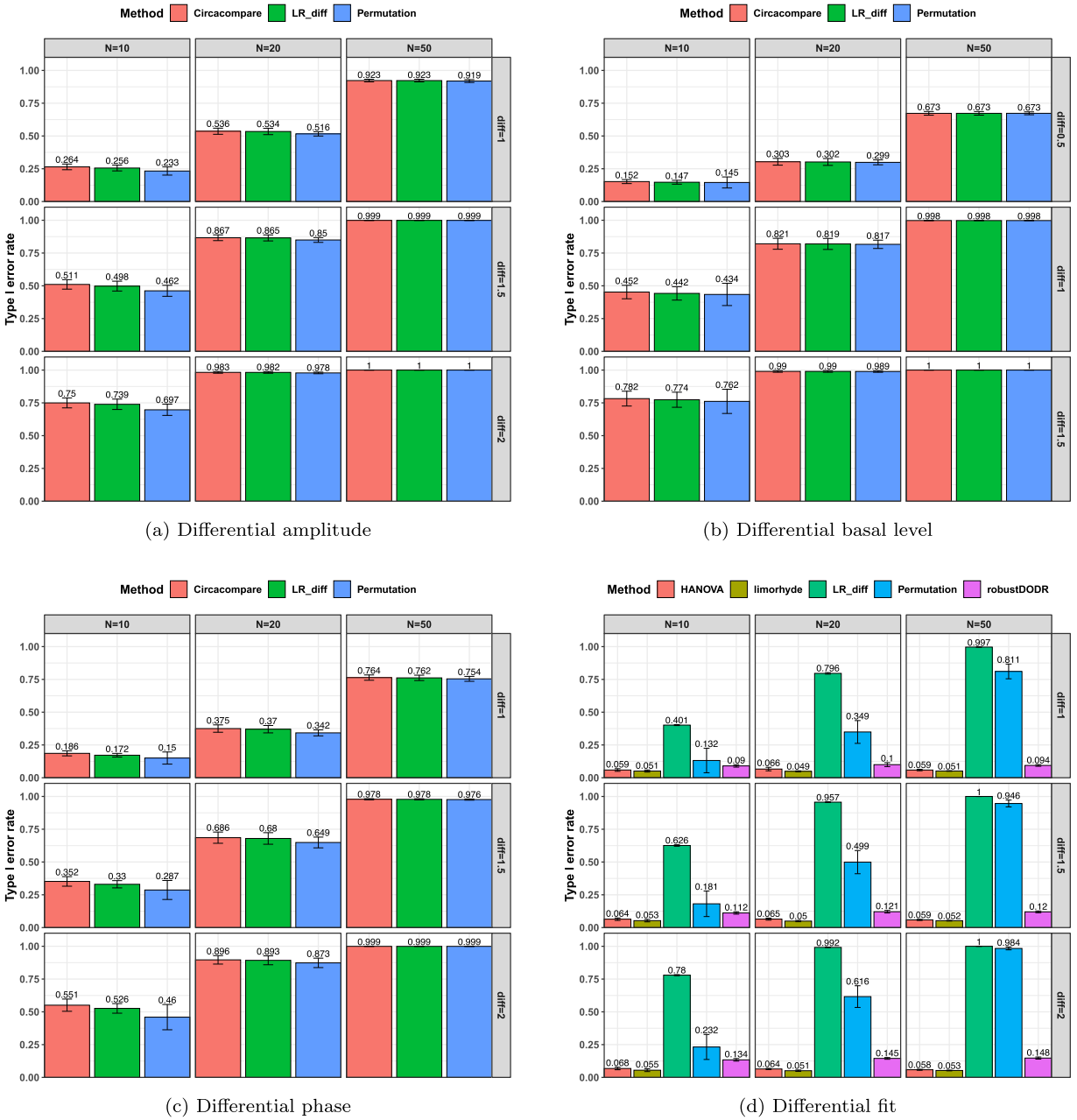

(a) Differential amplitude

(b) Differential basal level

(c) Differential phase

(d) Differential fit

FIGURE 5. Power evaluation for six different methods in detecting differential circadian patterns. The differential circadian patterns include differential amplitude, differential phase, differential basal level and differential fit. The sample sizes were varied at N=10, 20 and 50. The standard deviation of the mean type I error rate was also marked on the bar plot.

(comparing time-restricted feeding [i.e. restricted versus unrestricted]), a gene expression RNA sequencing data of mouse skeletal muscles (comparing exercise status [i.e. exercise group versus sedentary group]) and a single cell RNA sequencing data of mouse suprachiasmatic nucleus (no comparison groups). Throughout this section, we used $P \leq 0.01$ as the cutoff to declare statistical significance unless otherwise specified. Since our likelihood-based method includes both circadian rhythmicity P-values and differential circadian pattern P-values, we denote p_c as a P-value for circadian rhythmicity detection (i.e. from LR_rhythmicity), and p_d as a P-value for differential circadian pattern analysis i.e. from LR_diff). p_d can also be expanded as $p_d^{(a)}$ (differential amplitude); $p_d^{(p)}$ (differential phase); $p_d^{(c)}$ (differential basal level); $p_d^{(f)}$ (differential fit). We did not systematically compare our methods with existing methods in the real data application, because there is no underlying truth in the real data, and thus it is difficult to benchmark their performance.

Human brain aging data

We first examined our methods in a transcriptomic profile in a human postmortem brain data (Brodmann's area 11 in the prefrontal cortex). Detailed description of this study has been previously described by Chen *et al.* [4]. The final samples included 146 individuals whose time of death (TOD) could be precisely

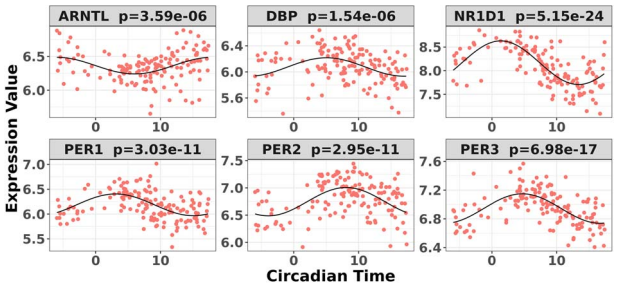

FIGURE 6. Circadian rhythmicity for six core circadian genes in the brain aging data, including *PER1*, *PER2*, *PER3*, *ARNTL*, *NR1D1* and *DBP*, using LR_rhythmicity.

determined. The mean age at death was 50.7 years; 78% of the individuals were male, and the mean postmortem interval was 17.3 hours. The TODs were further adjusted as the Zeitgeber time (ZT), which adjusted factors including time zone, latitude, longitude and altitude. The ZT was used as the circadian time, which was comparable across all individuals. A total of 33 297 gene probes were available in this microarray data, which was publicly available in GEO (GSE71620). After filtering 50% gene probes with lower mean expression level, 16 648 gene probes remained in the analysis.

Circadian rhythmicity detection

Under $p_c \leq 0.01$, we detected 528 significant circadian genes using LR_rhythmicity. Figure 6 shows the six core circadian genes, including *PER1*, *PER2*, *PER3*, *ARNTL*, *NR1D1* and *DBP*, which are known to have persistent circadian rhythmicity. All these six circadian genes rendered significant *P*-values ($5.15 \times 10^{-24} \sim 3.59 \times 10^{-6}$), showing the good detection power of our method in identifying circadian patterns. The number of significant circadian genes using other methods is shown in Table S2. We further performed pathway enrichment analysis. Using pathway analysis $P \leq 0.01$ as cutoff, LR_rhythmicity detected four pathways. The most significant pathway was the circadian rhythm signaling pathway ($P = 3.16 \times 10^{-6}$). The second most significant pathway was the senescence pathway ($P = 4.27 \times 10^{-4}$), which was also known to be associated with circadian oscillation [20].

Differential circadian analysis

In order to examine whether the chronological age was associated with disruption of circadian patterns, we further performed differential circadian analysis comparing the young group and the old group using our likelihood-based method. We first divided the 146 individuals into two groups: young group (age ≤ 40, n=31) and old group (age > 60, n=37). Under $p_c \leq 0.01$, we identified 205 genes showing circadian rhythmicity in young group and 164 genes in old group, with a total of 363 unique genes, and 6 common genes.

In terms of differential fit, we started with 363 candidate genes that showed circadian rhythmicity ($p_c \leq 0.01$) in either young or old. Comparing the old group to the young group (baseline group), LR_diff identified six genes showing differential fit ($p_d^{(f)} \leq 0.01$). As shown in Figure 1d, *MYO5A* is the gene showing most differential fit ($p_d^{(f)} = 4.34 \times 10^{-8}$), where there was circadian rhythmicity in the young group, but not in the old group. In terms of differential amplitude, differential phase and differential basal level, we started with six candidate genes that showed circadian rhythmicity ($p_c \leq 0.01$) in both young and old groups. Comparing the old group to the young group (baseline group), our likelihood-based method identified one gene showing differential amplitude ($p_d^{(a)} \leq 0.01$), four genes showing differential phase ($p_d^{(p)} \leq 0.01$) and two genes showing differential basal level ($p_d^{(b)} \leq 0.01$). Figure 1A– 1C showed the most significant genes in terms of differential amplitude (*CIART*, $P = 0.008$), differential phase (*PER2*, $P = 5.43 \times 10^{-5}$) and basal level (*TRIB2*, $P = 2.88 \times 10^{-6}$) comparing young and old groups, respectively.

Due to the small sample size and relatively weak transcriptomic alterations in brain tissues, the number of candidate genes for differential circadian analysis was small. Thus, we further relaxed the criteria to be $p_c \leq 0.05$, and we identified 897 rhythmic genes in the young group and 846 rhythmic genes in the old group. In terms of differential fit, among 1688 genes that showed circadian rhythmicity ($p_c \leq 0.05$) in either young or old group, LR_diff identified 345 genes showing gain or loss of rhythmicity. In terms of differential amplitude, differential phase and differential basal level, we started with 55 candidate genes that showed circadian rhythmicity ($p_c \leq 0.05$) in both young and old groups. Comparing the old group to the young group (baseline group), LR_diff identified 2 genes showing differential amplitude, 23 genes showing differential phase and 19 genes showing differential basal level.

Human time-restricted feeding data

We evaluated the performance of our likelihood-based methods in transcriptomic profiles of mouse skeletal muscle tissue. Eleven overweight or obese men were included in this dataset; the age range was 30–45 years; the body mass index range was 27–35 kg/m^2. These participants were randomized into time-restricted feeding (TRF) group and the un-restricted feeding (URF) group by adopting a cross over design, where each participant was assigned to both TRF and URF groups in different time periods. The skeletal muscle samples of each participant under each experimental group were repeatedly measured every 4 hours over 24 hours. There were some missing measurement, but each participant had $4 \sim 6$ measurement, resulting in a total of 63 samples in restricted group and 62 samples in unrestricted group. Detailed description of this study has been previously published [24]. This RNA-seq dataset is publicly available in GEO (GSE129843). After filtering the genes with mean cpm less than 1, 13 167 gene probes remained for further analysis. We further performed log2 transformation (i.e. $\log 2(x+1)$, where x is the cpm of a gene in a sample) to improve the normality of the data.

Circadian pattern detection

We first applied the LR_rhythmicity method to this time-restricted feeding dataset. Under $p_c \leq 0.01$, we identified 1407 and 935 genes showing significant circadian rhythmicity for the restricted group and the unrestricted group, respectively. Figure S15 and S16 shows the six core circadian genes in the TRF group and the URF group, including *PER1*, *PER2*, *PER3*, *ARNTL*, *NR1D1* and *DBP*, which are known to have persistent circadian rhythmicity. For these six circadian genes for the restricted group and the unrestricted group, our method (LR_rhythmicity) yielded highly significant *P*-values ($1.35 \times 10^{-8} \sim 1.65 \times 10^{-21}$), showing the strong detection power of circadian rhythmicity. The number of significant circadian genes using other methods is shown in Table S2. We further performed pathway enrichment analysis. Using $p_{pathway} \leq 0.01$ as cutoff, our likelihood methods detected 61 and 105 significant pathways for the TRF group

and URF group, respectively. The top pathways enriched in both groups included circadian rhythm signaling pathway, prolactin signaling pathway and IGF-1 signaling pathway; both these pathways are related with circadian rhythmicity [6, 27].

Differential circadian analysis

We further performed differential circadian analysis comparing TRF and URF groups using LR_diff. In terms of differential fit, we started with candidate genes that showed circadian rhythmicity ($p_c \leq 0.01$) in either restricted or unrestricted (n=1864). Comparing the TRF group to the URF group (baseline group), LR_diff identified 57 genes showing differential fit ($p_d^{(f)} \leq 0.01$). The most significant gene, *RUFY1*, is shown in Figure S17D, where there was a rhythmicity in the TRF group but not in the URF group.

In terms of differential amplitude, differential phase and differential basal level, we started with candidate genes that showed circadian rhythmicity ($p_c \leq 0.01$) in both TRF and URF (n=478). Comparing TRF to URF, 11 genes showing differential amplitude ($p_d^{(a)} \leq 0.01$), 25 genes showing differential phase $p_d^{(p)} \leq 0.01$ and 8 genes showing differential basal level $p_d^{(b)} \leq 0.01$. Figure S17A–C showed the most significant genes for differential amplitude, phase and basal level comparing TRF and URF groups, respectively.

Mouse exercise data

We further evaluated the performance of our proposed methods in an RNA-seq gene expression profile generated from mouse skeletal muscle. A total of 69 mice samples were collected, which can be divided to the sedentary group and exercise group (acute treadmill exercise). Skeletal muscles were harvested after 0, 4, 8, 12, 16 and 20 hours after sedentary or exercise treatment. Detailed description of this study has been previously published [32]. This RNA-seq dataset is publicly available in GEO (GSE126962). With 11 461 gene probes after filtering, we performed log2 transformation [i.e. $\log 2(x+1)$, where x is the cpm of a gene in a sample] to improve the normality of the data.

Circadian pattern detection

We first applied the LR_rhythmicity method to this mouse exercise dataset. Under $p_c \leq 0.01$, we identified 621 and 752 genes showing significant circadian rhythmicity for the sedentary group and the exercise group, respectively. Figures S18 and S19 show the six core circadian genes in the sedentary group and the exercise group, including *Per1*, *Per2*, *Per3*, *Arntl*, *Nr1d1* and *Ddp*, which are known to have persistent circadian rhythmicity. For these six circadian genes for the sedentary group and the exercise group, our method (LR_rhythmicity) obtained highly significant *P*-values ($6.76 \times 10^{-5} \sim 2.23 \times 10^{-17}$), demonstrating the strong detection power of circadian rhythmicity. The number of significant circadian genes using other methods is shown in Table S2. Using $p_{pathway} \leq 0.01$ as cutoff, our likelihood methods detected 25 and 63 significant pathways for the sedentary group and exercise group, respectively. We further performed pathway enrichment analysis and found that the circadian rhythm signaling pathway is the top pathway for both the sedentary group and the exercise group. In addition, the NRF2-mediated oxidative stress response pathway was very significant in the exercise group ($P = 3.2 \times 10^{-8}$), but much less significant in the sedentary group ($P = 0.002$). This is consistent with the literature that Nrf2 pathway plays important roles in mediating oxidative stress after acute exercise [8].

Differential circadian analysis

We further performed differential circadian analysis comparing sedentary and exercise groups using LR_diff. In terms of differential fit, we started with candidate genes that showed circadian rhythmicity ($p_c \leq 0.01$) in either sedentary or exercise (n=1060). Comparing the exercise group to the sedentary group (baseline group), LR_diff identified 32 genes showing differential fit ($p_d^{(f)} \leq 0.01$). The most significant gene, *Maff*, is shown in Figure S20D, where there was a rhythmicity in the exercise group but not in the sedentary group. In terms of differential amplitude, differential phase and differential basal level, we started with candidate genes that showed circadian rhythmicity ($p_c \leq 0.01$) in both sedentary and exercise groups (n=313). Comparing the exercise group to the sedentary group, four genes showing differential amplitude ($p_d^{(a)} \leq 0.01$), 10 genes showing differential phase $p_d^{(p)} \leq 0.01$ and 33 genes showing differential basal level $p_d^{(b)} \leq 0.01$. Figure S20A–C showed the most significant genes for differential amplitude, phase and basal level comparing sedentary and exercise groups, respectively.

Mouse single-cell RNA Sequencing (scRNAseq) data

In mammals, the suprachiasmatic nucleaus (SCN) is considered as the master pacemaker to overarch prepheriphal circadian clocks. To examine circadian pattern at single cell level in SCN, we applied the LR_rhythmicity algorithm in a mouse SCN scRNAseq data. The scRNAseq data are publicly available under GSE117295, and detailed descriptions about these data were described elsewhere [42]. To be brief, mice were housed in a 12 hour light:dark cycle for 2 weeks, followed by 2 days constant darkness. During the constant darkness period, these mice were separately sacrificed at 12 circadian time points (CT14, CT18,... CT58). A total of 62 071 cells from all 12 mouse samples were pooled together for data analysis. After applying the following filtering procedures: (i) cells with less than 200 genes were removed; (ii) dead cells with less than 5% mitochondrial genes detection ratio were removed, 59 803 cells remained and were used for clustering analysis. The data were further normalized using the LogNormalize method with a scale factor 10,000. Top 2000 highly variable genes were identified using the *vst* method of the Seurat package [37], followed by principal component analysis. Cell clustering analysis was performed by using a graph-based local moving algorithm [41]. To visualize the clusters in a 2-dimensional plot, we performed dimension reduction via t-distributed stochastic neighbor embedding [40]. Eighteen clusters were identified, which were further merged into seven unique cell types (Figure S21) after comparing brain cell signature genes [42]. Number of cells for each cell type is shown in Figure S22A. For each of these seven cell types, we performed the LR_rhythmicity analysis to detect genes with circadian rhythmicity, respectively.

Circadian pattern detection

As shown in Figure S22B, under $p_c \leq 0.01$, neurons had the most number of circadian genes (n=4658), followed by oligodendrocytes (n=2219), ependymocytes (n=1431), astrocytes (n=1156), endothelials (n=1044), NG2_cells (n=760) and microglia (n=458). A total of 28 genes showed circadian rhythmicity pattern across all these seven cell types. Figure S23 shows the core circadian genes (*Arntl*, *Dbp*, *Nr1d1*, *Per1*, *Per2* and *Per3*) by cell types. We found *Dbp* (*P*-values ranged from $6.67 \times 10^{-158} \sim 8.17 \times 10^{-9}$) and *Per3* (*P*-values ranged from $1.08 \times 10^{-18} \sim 1.84 \times 10^{-3}$)

showed circadian rhythmicity in all seven cell types. Interestingly, *Arntl* showed circadian rhythmicity pattern in ependymocytes, endothelials, neurons and NG2_cells (*P*-values ranged from $1.30 \times 10^{-15} \sim 3.93 \times 10^{-3}$), but not in astrocytes, microglia or oligodendrocytes (*P*-values ranged from $0.012 \sim 0.706$), indicating a potential cell type specific circadian rhythmicity pattern for *Arntl* in mouse SCN.

DISCUSSION

In summary, we developed a series of likelihood-based methods for detecting (i) circadian rhythmicity and (ii) differential circadian patterns. In terms of circadian rhythmicity detection, our method (LR_rhythmicity) could better control the type I error rate to its nominal level (i.e. produce an accurate *P*-values) than the other competing methods. In terms of differential circadian patterns, our likelihood-based method is the first parametric method to characterize four subcategories of differential circadian patterns, including differential amplitude, differential phase, differential basal level and differential fit. Simulation shows that our method (LR_diff) successfully controlled the type I error rate to the 5% nominal level for all four types of differential circadian patterns under the Gaussian assumption. In addition, LR_diff was more powerful than the competing methods in terms of differential fit. We also applied our methods in transcriptomic data applications including a human brain aging gene expression microarray data, a human time restricted feeding data, a mouse exercise RNA sequencing data, and a mouse SCN single cell RNA sequencing data. Superior performance has been observed in these applications.

Our methods have the following strengths. (i) The type I error rates of both LR_rhythmicity and LR_diff were well controlled, indicating the *P*-values from these methods are accurate. While in the literature, it remained a concern about the type I error rate control for existing methods in terms of detecting circadian rhythmicity. (ii) Some methods require integer input circadian time, and even intervals between adjacent circadian time, while our methods have no such restrictions. Circadian time from modern epidemiology studies usually unevenly distributed between 0 hours and 24 hours. Thus, our method can be more applicable in biomedical applications. (iii) For examining differential fit, our method is statistically more powerful compared to other existing methods. (iv) LR_rhythmicity is robust against the violation of the Gaussian assumptions. As shown in our simulation, the severe violation of the Gaussian assumptions will only result in slightly smaller than expected type I error rate. We feel that being slightly conservative is not a bad thing because this won't contribute false positive results.

Our methods could potentially suffer from the following limitation. Our proposed methods are based on likelihood, which assume the residuals (i.e. $y_i - \hat{y}_i$) are normally distributed. The violation of the Gaussian assumptions may result in an inflated/deflated type I error rate for some of our methods. In this case, we would recommend users to check the normality assumptions of the residuals. If the residuals violated the Gaussian assumption, we would recommend data transformations (e.g. Box–Cox transformation) before applying our method. We have included a concrete example to show how to use the Box–Cox transformation to rescue the normality assumption in Supplementary Material Section 1.

We plan to do the following future works. (i) In epidemiology studies, many other biological factors (e.g. age, gender, etc.) could have a confounding impact on the circadian rhythmicity. Adjusting for covariates may potentially improve parameter estimations and biological interpretations. Our likelihood-based framework is capable of being extended to adjust for covariates. (ii) To the best of our knowledge, no circadian rhythmicity detection method could handle repeated measurement from the same individuals. For example, the time restricted feeding data example employed a cross-over design, and the 11 participants with each participant repeatedly measured four to six times. By extending our methods to model this within subject correlation, we would expect higher power to detect circadian rhythmicity and differential circadian patterns. An R package for our method is publicly available on GitHub https://github.com/diffCircadian/diffCircadian.

Key Points

- Systematically evaluated the accuracy of *P*-values in detecting circadian rhythmicity of our likelihood-based methods and other existing methods.
- The first to propose likelihood-based methods to identify four subcategories of differential circadian patterns.
- Systemically evaluated our likelihood-based methods in detecting differential circadian patterns, and compared with existing methods in terms of the correctness of *P*-value and statistical power.
- Implemented our proposed methods in R software package, which has been made publicly available on GitHub.

Supplementary Data

Supplementary data are available online at *Briefings in Bioinformatics*.

Acknowledgments

We thank the anonymous reviewers for their valuable suggestions.

Funding

H.D., L.M., K.E., Z.H. are supported by the National Institutes of Health grants R01HL153042 and R01AR079220; C.M. and G.T. are supported by the National Institutes of Health grant R01MH111601.

References

1. Badia P, Myers B, Boecker M, *et al*. Bright light effects on body temperature, alertness, EEG and behavior. *Physiol Behav* 1991; **50**(3): 583–8.
2. Box GEP, Cox DR. An analysis of transformations. *J R Stat Soc B Methodol* 1964; **26**(2): 211–43.
3. Cagnacci A, Elliott JA, Yen SS. Melatonin: a major regulator of the circadian rhythm of core temperature in humans. *J Clin Endocrinol Metabol* 1992; **75**(2): 447–52.
4. Chen C-Y, Logan RW, Ma T, *et al*. Effects of aging on circadian patterns of gene expression in the human prefrontal cortex. *Proc Natl Acad Sci* 2016; **113**(1): 206–11.

5. Cornelissen G. Cosinor-based rhythmometry. *Theor Biol Med Model* 2014; **11**(1): 16.
6. Crosby P, Hamnett R, Putker M, *et al*. Insulin/igf-1 drives period synthesis to entrain circadian rhythms with feeding time. *Cell* 2019; **177**(4): 896–909.
7. Dijk D-J, Duffy JF, Czeisler CA. Circadian and sleep/wake dependent aspects of subjective alertness and cognitive performance. *J Sleep Res* 1992; **1**(2): 112–7.
8. Done AJ, Traustadóttir T. Nrf2 mediates redox adaptations to exercise. *Redox Biol* 2016; **10**:191–9.
9. Elzhov TV, Mullen KM, Spiess A-N, *et al*. *minpack.lm: R Interface to the Levenberg–Marquardt Nonlinear Least-Squares Algorithm Found in MINPACK, Plus Support for Bounds*, 2016. R package version 1:2–1.
10. Glynn EF, Chen J, Mushegian AR. Detecting periodic patterns in unevenly spaced gene expression time series using Lomb–Scargle periodograms. *Bioinformatics* 2006; **22**(3): 310–6.
11. Hastings MH, Brancaccio M, Maywood ES. Circadian pacemaking in cells and circuits of the suprachiasmatic nucleus. *J Neuroendocrinol* 2014; **26**(1): 2–10.
12. Hodge BA, Wen Y, Riley LA, *et al*. The endogenous molecular clock orchestrates the temporal separation of substrate metabolism in skeletal muscle. *Skelet Muscle* 2015; **5**(1): 17.
13. Hsu PY, Harmer SL. Circadian phase has profound effects on differential expression analysis. *PLoS One* 2012; **7**(11): e49853.
14. Hughes ME, Abruzzi KC, Allada R, *et al*. Guidelines for genome-scale analysis of biological rhythms. *J Biol Rhythms* 2017; **32**(5): 380–93.
15. Hughes ME, DiTacchio L, Hayes KR, *et al*. Harmonics of circadian gene transcription in mammals. *PLoS Genet* 2009; **5**(4): e1000442.
16. Hughes ME, Hogenesch JB, Kornacker K. Jtk_cycle: an efficient nonparametric algorithm for detecting rhythmic components in genome-scale data sets. *J Biol Rhythms* 2010; **25**(5): 372–80.
17. Hughey JJ, Butte AJ. Differential phasing between circadian clocks in the brain and peripheral organs in humans. *J Biol Rhythms* 2016; **31**(6): 588–97.
18. Hurley JM, Loros JJ, Dunlap JC. Circadian oscillators: around the transcription–translation feedback loop and on to output. *Trends Biochem Sci* 2016; **41**(10): 834–46.
19. Jung CM, Khalsa SBS, Scheer FAJL, *et al*. Acute effects of bright light exposure on cortisol levels. *J Biol Rhythms* 2010; **25**(3): 208–16.
20. Kunieda T, Minamino T, Katsuno T, *et al*. Cellular senescence impairs circadian expression of clock genes in vitro and in vivo. *Circ Res* 2006; **98**(4): 532–9.
21. Laloum D, Robinson-Rechavi M. Methods detecting rhythmic gene expression are biologically relevant only for strong signal. *PLoS Comput Biol* 2020; **16**(3): e1007666.
22. Li JZ, Bunney BG, Meng F, *et al*. Circadian patterns of gene expression in the human brain and disruption in major depressive disorder. *Proc Natl Acad Sci* 2013; **110**(24): 9950–5.
23. Lim ASP, Klein H-U, Yu L, *et al*. Diurnal and seasonal molecular rhythms in human neocortex and their relation to Alzheimer's disease. *Nat Commun* 2017; **8**(1): 1–16.
24. Lundell LS, Parr EB, Devlin BL, *et al*. Time-restricted feeding alters lipid and amino acid metabolite rhythmicity without perturbing clock gene expression. *Nat Commun* 2020; **11**(1): 1–11.
25. Mei W, Jiang Z, Chen Y, *et al*. Genome-wide circadian rhythm detection methods: systematic evaluations and practical guidelines. *Briefings in Bioinformatics*. 2021; **22**(3): bbaa135.
26. Möller-Levet CS, Archer SN, Bucca G, *et al*. Effects of insufficient sleep on circadian rhythmicity and expression amplitude of the human blood transcriptome. *Proc Natl Acad Sci* 2013; **110**(12): E1132–41.
27. Morris CJ, Aeschbach D, Scheer FAJL. Circadian system, sleep and endocrinology. *Mol Cell Endocrinol* 2012; **349**(1): 91–104.
28. Parker T. Finite-sample distributions of the Wald, likelihood ratio, and Lagrange multiplier test statistics in the classical linear model. *Commun Stat Theory Methods* 2017; **46**(11): 5195–202.
29. Parsons R, Parsons R, Garner N, *et al*. Circacompare: a method to estimate and statistically support differences in mesor, amplitude and phase, between circadian rhythms. *Bioinformatics* 2020; **36**(4): 1208–12.
30. Pelikan A, Herzel H, Kramer A, *et al*. Studies overestimate the extent of circadian rhythm reprogramming in response to dietary and genetic changes. *bioRxiv*, 2020.
31. Ruben MD, Wu G, Smith DF, *et al*. A database of tissue-specific rhythmically expressed human genes has potential applications in circadian medicine. *Sci Transl Med* 2018; **10**(458).
32. Sato S, Basse AL, Schönke M, *et al*. Time of exercise specifies the impact on muscle metabolic pathways and systemic energy homeostasis. *Cell Metab* 2019; **30**(1): 92–110.
33. Seney ML, Cahill K, Enwright JF, *et al*. Diurnal rhythms in gene expression in the prefrontal cortex in schizophrenia. *Nat Commun* 2019; **10**(1): 1–11.
34. Singer JM, Hughey JJ. Limorhyde: a flexible approach for differential analysis of rhythmic transcriptome data. *J Biol Rhythms* 2019; **34**(1): 5–18.
35. Stenvers DJ, Jongejan A, Atiqi S, *et al*. Diurnal rhythms in the white adipose tissue transcriptome are disturbed in obese individuals with type 2 diabetes compared with lean control individuals. *Diabetologia* 2019; **62**(4): 704–16.
36. Straume M. DNA microarray time series analysis: automated statistical assessment of circadian rhythms in gene expression patterning. *Methods in Enzymology* 2004; **383**: 149–66.
37. Stuart T, Butler A, Hoffman P, *et al*. Comprehensive integration of single-cell data. *Cell*. 2019; **177**(7): 1888–902.
38. Thaben PF, Westermark PO. Detecting rhythms in time series with rain. *J Biol Rhythms* 2014; **29**(6): 391–400.
39. Thaben PF, Westermark PO. Differential rhythmicity: detecting altered rhythmicity in biological data. *Bioinformatics* 2016; **32**(18): 2800–8.
40. van der Maaten L, Hinton G. Visualizing data using t-sne. *J Mach Learn Res* 2008; **9**(86): 2579–605.
41. Waltman L, van Eck NJ. A smart local moving algorithm for large-scale modularity-based community detection.*The European physical journal B*. 2013; **86**(1): 1–4.
42. Ma D, Zhao M, Xie L, *et al*. Spatiotemporal single-cell analysis of gene expression in the mouse suprachiasmatic nucleus. *Nature neuroscience*. 2020; **23**(3): 456–67.
43. Wu G, Anafi RC, Hughes ME, *et al*. Metacycle: an integrated r package to evaluate periodicity in large scale data. *Bioinformatics* 2016; **32**(21): 3351–3.
44. Yang R, Zhen S. Analyzing circadian expression data by harmonic regression based on autoregressive spectral estimation. *Bioinformatics* 2010; **26**(12): i168–74.
45. Ypma J. Introduction to nloptr: an r interface to nlopt. *R Package* 2014; **2**.
46. Zhang R, Lahens NF, Ballance HI, *et al*. A circadian gene expression atlas in mammals: implications for biology and medicine. *Proc Natl Acad Sci* 2014; **111**(45): 16219–24.